Available online at www.sciencedirect.com
ScienceDirect
Geochimica et Cosmochimica Acta 71 (2007) 2104–2119
Geochimica et Cosmochimica Acta
www.elsevier.com/locate/gca

Os, Pb, and Nd isotope geochemistry of the Permian Emeishan continental flood basalts: Insights into the source of a large igneous province

Ji-Feng Xu [a,*], Katsuhiko Suzuki [b,*], Yi-Gang Xu [a], Hou-Jun Mei [a], Jie Li [a]

[a] Key Laboratory of Isotope Geochronology and Geochemistry, Guangzhou Institute of Geochemistry, Chinese Academy of Sciences, 510640 Wushan, Guangzhou, China
[b] Institute for Research on Earth Evolution (IFREE), Japan Agency for Marine-Earth Science and Technology (JAMSTEC), 2–15 Natsushima, Yokosuka 237-0061, Japan

Received 15 May 2006; accepted in revised form 30 January 2007; available online 8 February 2007

Abstract

The nature of the source of continental flood basalts (CFB) is a highly debated topic. Proposed mantle sources for CFBs, including both high- and low-Ti basalts, include subcontinental lithospheric mantle (SCLM), asthenospheric mantle, and deep, plume-related mantle. Re–Os isotope systematics can offer important constraints on the sources of both ocean island basalts (OIB) and CFB, and may be applied to distinguish different possible melt sources. This paper reports the first Re–Os isotope data for the Late Permian Emeishan large igneous province (LIP) in Southwest China. Twenty one CFB samples including both low- and high-Ti basalts from five representative sites within the Emeishan LIP have been analyzed for Os, Nd, and Pb isotopic compositions. The obtained Os data demonstrate that crustal assimilation affected Os isotopic compositions of some Emeishan basalt samples with low Os concentrations but not all of the samples, and the Emeishan basalts with high Os contents likely experienced the least crustal contamination. The low and high-Ti basalts yield distinct Os signatures in terms of $^{187}Os/^{188}Os$ and Os content. The low-Ti basalt with the highest Os concentration (400 ppt) has a radiogenic Os isotopic composition ($\gamma Os(t)$, +6.5), similar to that of plume-derived OIB. Because the Os isotopic composition of basalts with relatively high Os concentrations (typically >50 ppt) likely represents that of their mantle source, this result implies a plume-derived origin for the low-Ti basalts. On the other hand, the high-Ti basalts with high Os concentration (over 50 ppt) have unradiogenic Os isotopic signatures ($\gamma Os(t)$ values range from −0.8 to −1.4), suggesting that a subcontinental lithosphere mantle (SCLM) component most likely contributed to the generation of these magmas. Combining Pb and Nd isotopic tracers with the Os data, we demonstrate that the low-Ti basaltic magmas in the Emeishan CFB were mainly sourced from a mantle plume reservoir, whereas the high-Ti basaltic magmas were most likely derived from a SCLM reservoir or were contaminated by a significant amount of lithospheric mantle material during plume-related magma ascent through the SCLM.

1. INTRODUCTION

Continental flood basalts (CFB) and oceanic island basalts (OIB) are commonly thought to represent melting products of mantle plumes. However, the nature of the source and the processes that produce plume-derived magmas are not well understood. Whether the primary source of CFB magmas is subcontinental lithospheric mantle (SCLM), shallow asthenospheric mantle or deep plume-related mantle is a highly debated topic. The Re–Os isotopic system is a potentially powerful tool for tracing the source and origin of magmas in continental settings. One of the reasons is that SCLM typically has lower Os isotopic compositions than the hypothetical primitive upper mantle, with $^{187}Os/^{188}Os$ ratio of 0.1296 (Meisel et al., 2001), whereas plume-related OIB-type mantle has higher Os

* Corresponding authors. Fax: +86 20 85290130 (J.-F. Xu).
E-mail addresses: jifengxu@gig.ac.cn (J.-F. Xu), katz@jamstec.go.jp (K. Suzuki).

0016-7037/$ - see front matter © 2007 Elsevier Ltd. All rights reserved.
doi:10.1016/j.gca.2007.01.027

isotopic compositions (e.g., $^{187}Os/^{188}Os$ ratios range from 0.13 to 0.15, Shirey and Walker, 1998). However, relative to OIBs, available Os isotopic data for CFBs are still few, with recently published data for only Karoo, Siberian, Ferrar and Columbia River provinces (Ellam et al., 1992; Horan et al., 1995; Molzahn et al., 1996; Chesley and Ruiz, 1998). The Re–Os isotopic compositions of high-Mg volcanic rocks among the Karoo and Siberian CFBs suggest that they were mainly derived from melting of a plume mantle with little involvement of the lithospheric mantle (Ellam et al., 1992; Horan et al., 1995). On the other hand, Re–Os isotopic compositions of the dominant basaltic lavas from continental large igneous provinces (LIPs) suggest that these basaltic melts were derived from distinct mantle sources: that an enriched SCLM component played an important role in the production of the Ferrar CFBs (Molzahn et al., 1996), whereas a SCLM source was not significantly involved in the formation of the Columbia River CFBs (Chesley and Ruiz, 1998). These studies show the potential of the Re–Os system to shed light on the sources of CFBs, and also that petrogenetic processes of the basaltic magmas may vary greatly from province to province and thus are still not well understood. In order to better understand CFB petrogenesis, it is necessary to increase the database of Re–Os and other isotope data on these rocks.

The Emeishan continental flood basalts in southwestern China are regarded as a LIP (Coffin and Eldholm, 1994; Chung et al., 1998; and Xu et al., 2001), and have been suggested to represent the melting products of a mantle plume (Campbell and Griffiths, 1990; Chung and Jahn, 1995; Xu et al., 2004). Although the plume model has been increasingly adopted to explain the generation processes of the Emeishan CFBs, doubts have been cast on the applicability of the model because the Emeishan LIP has a relatively small exposure (250,000 km^2) compared with typical LIPs (over 1,000,000 km^2, Coffin and Eldholm, 1994), as well as fewer volcanic cycles. In addition, the sources of the high-Ti and low-Ti basalts in the Emeishan LIP have been highly debated. Although some previous studies suggested that the Emeishan CFBs were products of a mantle plume (Chung and Jahn, 1995; Xu et al., 2001), others have more recently argued that only the high-Ti basalts originated from a mantle plume, with the low-Ti basalts derived from a SCLM source (Xiao et al., 2003a,b, 2004). Thus, the source and origin of the Emeishan CFBs remain unclear.

This paper presents the first Re–Os isotopic data for Emeishan CFBs, together with Pb and Nd isotopic and elemental data. The geochemical results are consistent with a plume origin for the Emeishan CFBs and the Os data further show that the low-Ti basaltic magmas were mainly derived from plume material, whereas a lithopsheric mantle component was significant in the generation of the high-Ti basalts.

2. GEOLOGICAL BACKGROUND

The Emeishan CFBs compose the largest volcanic province within China, and are distributed in the western Yangtze (South China), Songpan-Ganze and eastern Qiangtang terranes (Fig. 1) (Chung et al., 1998; Xu et al., 2001). The volcanic successions, tilted and fragmented by complex tectonic events during Meso–Cenozoic times, are exposed in a rhombic area of $\sim 2.5 \times 10^5$ km^2 (500×500 km) in association with numerous intrusive bodies of ultramafic/mafic to felsic composition. The volcanic sequence thickness ranges from ~5 km in the Bingchuan section (Fig. 1) in the southwestern part to several hundred meters at the eastern and northeast margin within the LIP. The average lava thickness of this LIP was estimated to be about 700 m and the entire volume of the Emeishan basalts to be $\sim 0.3 \times 10^6$ km^3 (Lin, 1985). Recent studies (Xiao et al., 2003a, c) show that the upper Permian Jinping basalts in the Yunnan Province are part of the Emeishan LIP, although they are located to the southwest of the Ailaoshan-Red River fault zone that was traditionally thought to be the southwest boundary of the LIP. Therefore, the Emeishan LIP most likely covered a larger area when the CFBs were erupted. A recent biostratigraphic and stratigraphic investigation has shown that starting in the early Permian, thick (>1 km) carbonate sequences were deposited as a response to extensive transgression and basin subsidence in the southwest. Later, basement uplift took place, suggesting rapid kilometer-scale doming, accompanied by crustal thinning, before emplacement of the Emeishan lavas (He et al., 2003).

The Emeishan CFB lavas show spatial and temporal variations. The basaltic lavas can be divided into two major groups: high-Ti ($TiO_2 > 2.5$ wt%, Ti/Y ratio >500) and low-Ti ($1.5 < TiO_2 < 2.5$ wt%; Ti/Y ratio <500) (Xu et al., 2001; Xiao et al., 2003a,c). Lavas of the high-Ti group occur as the predominant component in the upper succession, whereas lavas of the low-Ti group are confined to the lower volcanic successions (Xu et al., 2001). The low-Ti lavas are exposed only in the southwest part of the province, including the low-Ti basalts recently recognized in the Jinping area (Xiao et al., 2003a). In contrast, the high-Ti lavas are found across almost the entire province. Locally, thick piles of trachyte and/or rhyolite form an important member in the upper sequence. Although small in volume, a few picrites have been recognized in the LIP (Chung and Jahn, 1995). In addition, there are numerous intrusive bodies exposed, ranging from ultramafic and mafic to felsic compositions and some of the mafic bodies are associated with large V–Ti–Fe ore deposits (Chung et al., 1998; Lin, 1985; Huang and Opdyke, 1998). Gabbros and syenites from intrusive complexes possess geochemical and Sr–Nd isotopic compositions comparable to those of the nearby basalts and trachytes–rhyolites (Chung et al., 1998; Lo et al., 2002), strongly suggesting a genetic link between the intrusive and volcanic rocks of the Emeishan LIP (Chung et al., 1998; Xu et al., 2001).

The exact timing of the main eruption of the Emeishan CFBs is still a debated topic. The Emeishan CFB successions unconformably overlie the early Late Permian Maokou Formation (composed mainly of marine limestones corresponding to the Capitanian/Kazanian stage) and underlie lower Triassic clastic sedimentary rocks. These biostratigraphic and stratigraphic constraints indicate that the CFBs were erupted during late Permian-early Triassic times. ^{40}Ar–^{39}Ar isotopic dates (Boven et al., 2002) indicate

a minimum apparent age of 246 ± 4 Ma for plagioclase from a plagiogranite, a late-differentiate of the Panzhihua Layered Complex, and an age of 254 ± 5 Ma for phlogopite from a pyroxenite in the Emeishan LIP. SHRIMP U/Pb zircon dating was carried out for two gabbro-peridotite intrusions, yielding crystallization ages of 258.7 ± 1.5 and 256.0 ± 1.0 Ma (Zhou et al., 2002). Other high-precision $^{40}Ar/^{39}Ar$ dating results for volcanic and intrusive rocks from the Emeishan LIP have defined the eruptive stage of flood magmatism at ~251 to 253 Ma (Lo et al., 2002), which is roughly synchronous with that of the Siberian traps (250 ± 1 Ma, Renne et al., 1995; 251 Ma, Kamo et al., 2003). Consequently, we believe that the Emeishan CFBs erupted between 251 and 259 Ma based on the above dating results.

3. SAMPLE DESCRIPTION AND ANALYTICAL METHODS

All samples studied here are basalts, collected from five sites (Fig. 1) within the Emeishan LIP: Binchuan, Jinping, Longzhoushan, Jinding, and Zhijin. The Binchuan and Jinping areas are located in the southwest part of the province, where both high and low-Ti lavas are associated, the latter

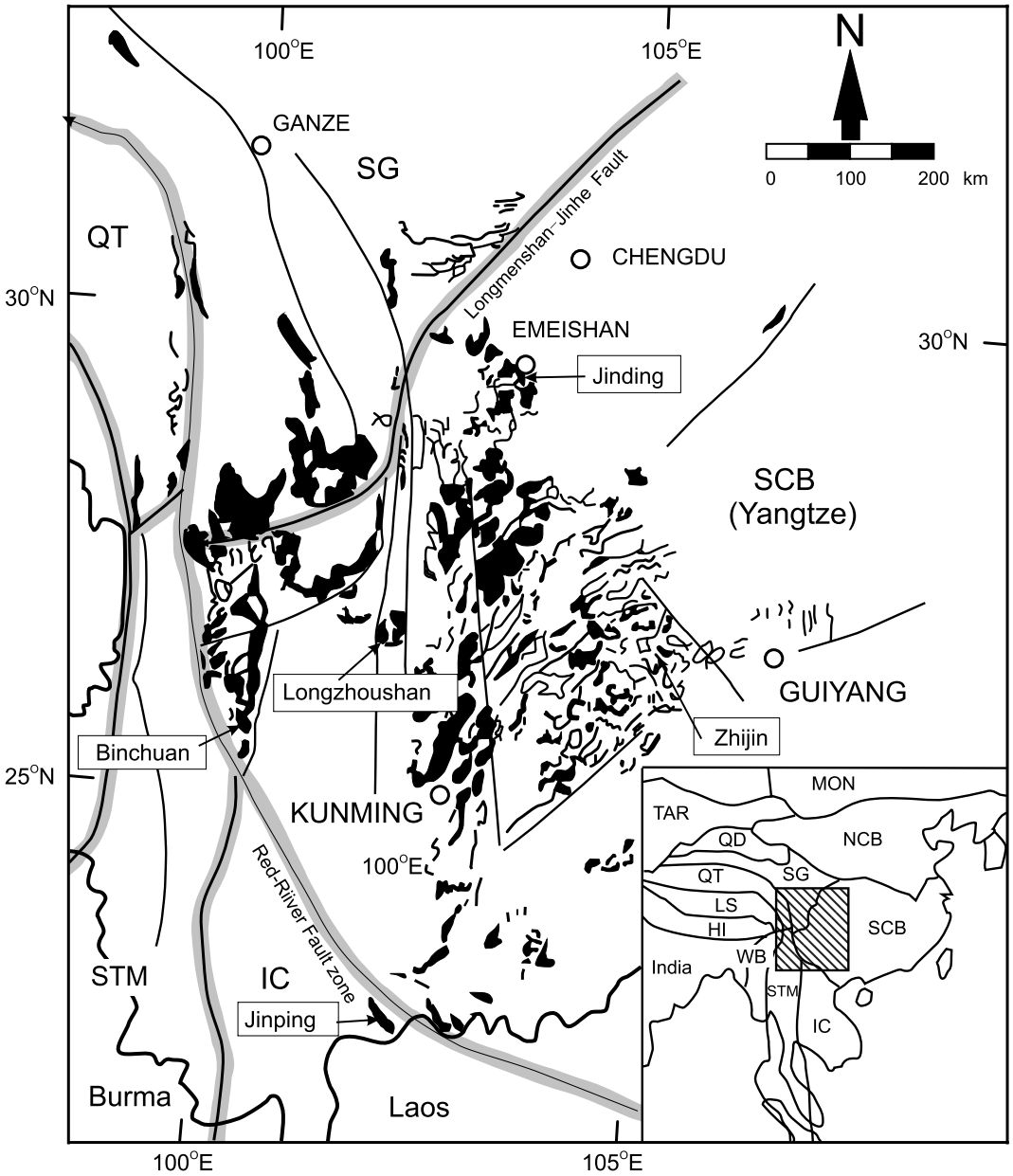

Fig. 1. Schematic map showing the distribution of the Permian–Triassic volcanic successions (black areas) within the Emeishan continental flood basalt province (modified after Xu et al., 2001). Site names with arrows indicate locations of samples collected in this study. The inset illustrates major tectonic units in eastern Asia. Major terranes: SCB, South China Block; SG, Songpan-Ganze Accretionary Complex; QT, Qiangtang; STM, Shan-Thai-Malay; IC, Indochina; WB, West Burma; HI, Himalayan; LS, Lhasa; QD, Qaidam; TAR, Tarim; MON, Mongolia; NCB, North China Block.

generally occur in the lower part of the volcanic succession. The Longzhoushan area is near the center, the Jinding area in the Emeishan Mountain is in the northeast part, and the Zhijin area is in the eastern part of the province. Only high-Ti lavas have been observed in the Longzhoushan, Jinding and Zhijin volcanic profiles. Most basaltic samples in this study are subaerial-vocanic rocks and are rather fresh except for several low-Ti basalts in the southwest part that are variably altered.

For Re–Os isotopic measurement, rock samples were first split into small chips using a hammer wrapped in paper to avoid contamination. The chips were then soaked in 4 hydrochloric acid for half an hour. After rinsing in distilled water, selected rock chips were powdered in an agate mortar by hand. This produced 5–10 g of powder for each sample. The analytical procedure is described in detail in Kato et al. (2005) and Suzuki and Honda (2003). Briefly, Os and Re concentrations and Os isotopic measurements were made on bulk samples using 1–3 g of powder. Samples were spiked with solutions enriched in ^{190}Os and ^{185}Re and digested in reverse *aqua regia* (2:1 HNO_3: HCl) in Carius tubes (Shirey and Walker, 1995). Osmium was extracted by carbon tetrachloride solvent extraction (Cohen and Waters, 1996; Pearson and Woodland, 2000) and further purified by micro distillation (Roy-Barman, 1993). Rhenium was extracted and purified from the remaining solution by anion exchange using AG 1×8 resin (100–200 mesh). Isotopic abundances of OsO_3^- and ReO_4^- were measured by negative thermal ionization mass spectrometry (Finnigan MAT 262) (Creaser et al., 1991; Volkening et al., 1991). All Re–Os isotopic compositions were determined at the Institute for Geothermal Sciences, Kyoto University, Japan. Osmium was measured by peak jumping on an electron multiplier. The peak on mass number 233, derived from Re background and possibly molecular interferences in the mass spectrometer and impurities in Pt filaments, was carefully checked during Os measurements, and the data with high intensities on mass 233 were not used for further calculations (Kato et al., 2005). From the measured oxide ratios, the isotopic ratios were calculated after correcting oxide interferences, instrumental mass fractionation and contributions from the ^{190}Os enriched spike. Instrumental mass fractionation for Os was corrected by normalizing the measured $^{192}Os/^{188}Os$ to 3.08271. Oxide corrections were made using $^{17}O/^{16}O = 0.00037$ and $^{18}O/^{16}O = 0.002047$ (Nier, 1950). Rhenium isotopic abundances were determined after total evaporation of the samples on the filaments (Suzuki et al., 2004). This method eliminates the effect of instrumental mass fractionation and yields isotopic ratios more accurate than conventional NTIMS measurement techniques. Total procedural blanks were ~7 pg for Re, and ~2 pg for Os with $^{187}Os/^{188}Os$ of ~0.298. Contribution of the blank to measured Os concentrations and $^{187}Os/^{188}Os$ were <10% and <5% respectively, except for a few samples with the low Os concentrations of ~7 ppt. Precision of $^{187}Os/^{188}Os$ measurements, based on analysis of an in-house standard over a period of several months, was better than 0.4% (two standard deviation). Standard errors ($2\ \sigma_m$) associated with the measured $^{187}Os/^{188}Os$ are given in Table 1.

For analysis of major and trace elements and Pb–Nd isotopes, the volcanic rock samples were first split into small chips and then soaked in 4 N hydrochloric acid for half an hour in order to leach out possible alteration minerals. The rock chips were powdered in an alumina ceramic shatterbox and the powders used for compositional analyses. Major elements were determined by gravimetry (wet chemistry) and X-Ray fluorescence (XRF), whereas trace element concentrations were measured using a PE Elan 6000 inductively-coupled plasma mass spectrometer (ICP-MS) at Guangzhou Institute of Geochemistry, Chinese Academy of Sciences. The analytical procedure for the ICP-MS analysis is similar to that described by Li (1997). Trace element concentrations were drift corrected using the standard sample BCR-1 (Li, 1997). Analytical uncertainties are generally less than 5–10%. Lead isotopic compositions were measured by thermal ionization mass spectrometry (TIMS) at Guangzhou Institute of Geochemistry, Chinese Academy of Sciences using a procedure similar to that described in Xu et al. (2002). Lead isotopic ratios were corrected for fractionation using replicate analyses of the standard NBS 981. Analytical uncertainties during the period of analysis were 0.006 for $^{206}Pb/^{204}Pb$ and $^{207}Pb/^{204}Pb$ and 0.012 for $^{208}Pb/^{204}Pb$. Nd isotopic compositions were measured using a Micromass Isoprobe multi-collector mass spectrometer (MC-ICPMS) also at the Guangzhou Institute of Geochemistry, Chinese Academy of Sciences. Analytical procedures were similar to those described in Wei et al. (2002) and Liang et al. (2003). The measured $^{146}Nd/^{144}Nd$ and fractionation-corrected $^{143}Nd/^{144}Nd$ ratios of the JNdi-1 standard were 0.710288 ± 28 ($2\sigma_m$) and 0.512109 ± 12 ($2\sigma_m$), respectively. All measured Nd isotopic ratios were normalized to $^{146}Nd/^{144}Nd = 0.71029$. Standard errors ($2\sigma_m$) of Pb and Nd isotope analyses are listed in Table 1.

4. RESULTS

In total, 21 basaltic samples from the Emeishan LIP were chosen for Os and Pb isotopic analysis (Table 1). Except for Binchuan and Jinping samples that had been previously analyzed for major and trace elements and Nd isotopes (Xiao et al., 2003a,b, 2004), Jinding, Longzhoushan and Zhijin basalts were measured in this study (Tables 1 and 2). These results, coupled with available published data, indicate that the samples may be divided into two groups: high-Ti and low-Ti basalt. The high-Ti basalts are characterized by relatively high TiO_2 contents (>2.5 wt%) and Ti/Y ratios (>500) as well as high LREE concentrations, whereas the low-Ti basalts have lower TiO_2 contents (<2.5 wt%), Ti/Y ratios (<500) and LREE concentrations (Xu et al., 2001) (seeing Table 1 and Fig. 2). In general, the low-Ti basalts also have higher $Mg^{\#}$ and lower $\varepsilon_{Nd}(t)$ compared to most high-Ti basalts. The Emeishan basaltic samples in this study show a relatively large variation in MgO (4.07–12.52 wt%), $Mg^{\#}$ (37–68) and Ni (20–263 ppm) (Table 1). Trace element variations correlate well with TiO_2 contents. For example, high-Ti basalts have steeper, LREE-enriched patterns than the low-Ti basalts (Fig. 2a and b) as well as generally higher LREE contents.

Table 1
Os, Pb and Nd isotopic compositions of the Emeishan continental flood basalts

	Rock type	Area	Ti/Y	Sm	Nd	$^{143}Nd/^{144}Nd$	±	εNd (255 Ma)	Re (ppb)	±	Os (ppb)	±	$^{187}Os/^{188}Os$	±
EMS-3	High-Ti basalt	Jinding	694	10.07	51.56	0.51258	(9)	1.4	0.476	(4)	0.1024	(13)	0.2205	(9)
Jd-3	High-Ti basalt	Jinding	705	10.02	49.73	0.51257	(11)	1.1	0.1717	(6)	0.00787	(4)	1.309	(6)
Jd-10	High-Ti basalt	Jinding	648	10.56	54.42	0.51262	(13)	2.2	0.2994	(15)	0.0554	(3)	0.2364	(5)
Fd-2	High-Ti basalt	Jinding	700						0.0968	(3)	0.0279	(2)	0.3071	(11)
Fd-3	High-Ti basalt	Jinding	715	10.08	50.86	0.51254	(9)	0.6	0.3359	(19)	0.01995	(10)	0.8430	(26)
Fd-7	High-Ti basalt	Jinding	717	10.79	54.58	0.51256	(10)	1.0	0.2773	(14)	0.0506	(4)	0.3283	(10)
Fd-10	High-Ti basalt	Jinding	777	10.40	51.92	0.51258	(13)	1.3	0.3785	(24)	0.0681	(6)	0.2619	(7)
WL-6	Low-Ti basalt	Binchuan	359	3.50	14.41	0.51254	(15)	−0.3	0.07561	(19)	0.400	(4)	0.1373	(6)
WL-12	Low-Ti basalt	Binchuan	372	3.85	16.02	0.51261	(12)	1.1	0.1654	(6)	0.1221	(11)	0.1663	(5)
WL-12-R	(Duplicate)								0.1730	(6)	0.1300	(7)	0.1745	(13)
WL-25	Low-Ti basalt	Binchuan	298	3.92	14.45	0.51252	(14)	−1.2	0.2307	(6)	0.00641	(8)	1.403	(19)
WL-33	Low-Ti basalt	Binchuan	434	3.60	14.14	0.51256	(11)	−0.1	0.06602	(17)	0.06287	(29)	0.1720	(4)
SC-2	Low-Ti basalt	Binchuan	371	4.55	19.42	0.51239	(12)	−3.1	0.3634	(13)	0.01108	(8)	0.918	(23)
RY-8	High-Ti basalt	Binchuan	702	5.07	18.51	0.51248	(15)	−0.7	0.06718	(16)	0.02445	(10)	0.262	(7)
JP-4	Low-Ti basalt	Jinping	385						0.10512	(26)	0.03945	(16)	0.2210	(10)
JP-8	Low-Ti basalt	Jinping	417	10.22	51.35	0.51235	(15)	−4.5	0.1746	(6)	0.0138	(4)	0.414	(9)
ZJ-6	High-Ti basalt	Zhijin	671	10.94	55.64	0.51261	(13)	2.0	0.2744	(8)	0.01935	(11)	0.503	(3)
LZ-1	High-Ti basalt	Longzhoushan	541	10.36	54.19	0.51228	(11)	−4.5	0.4612	(12)	0.00388	(4)	5.19	(4)
LZ-20	High-Ti basalt	Longzhoushan	446	8.06	39.30	0.51228	(9)	−4.7	0.1599	(4)	0.00498	(3)	1.215	(14)
LZ-50	High-Ti basalt	Longzhoushan	706	6.87	32.62	0.51260	(11)	2.0	0.03099	(8)	0.006857	(27)	0.4323	(28)
LZ-56	High-Ti basalt	Longzhoushan	703	9.96	54.28	0.51252	(14)	0.6	0.06602	(17)	0.560	(19)	0.1271	(3)
LZ-66	High-Ti basalt	Longzhoushan	1332	6.94	38.60	0.51252	(12)	0.3	0.1184	(3)	0.1035	(4)	0.1471	(10)

	$^{187}Re/^{188}Os$	±	$(^{187}Os/^{188}Os)_{255Ma}$	±	γOs (255Ma)	±	U (ppm)	Th (ppm)	Pb (ppm)	$^{238}U/^{204}Pb$	$^{232}Th/^{204}Pb$	$^{206}Pb/^{204}Pb$	±	$^{207}Pb/^{204}Pb$	±	$^{208}Pb/^{204}Pb$	±
EMS-3	22.7	(3)	0.1240	(17)	−1.1	1.4	1.41	6.1	7.26	12.5	56.0	18.724	(28)	15.61	(4)	39.35	(4)
Jd-3	120.4	(7)	0.797	(7)	536	6	1.34	5.33	6.55	13.4	55.2	19.417	(13)	15.660	(13)	39.891	(13)
Jd-10	26.41	(20)	0.1240	(10)	−1.0	0.8	1.4	6.12	7.12	12.8	57.7	18.84	(7)	15.64	(6)	39.63	(6)
Fd-2	17.13	(12)	0.2342	(12)	86.9	1.0	1.04	5.36	6.54	10.2	54.6	18.690	(19)	15.588	(18)	39.305	(17)
Fd-3	88.5	(7)	0.466	(4)	272	3	1.62	7.3	7.42	13.9	64.8	18.35	(8)	15.64	(8)	38.81	(9)
Fd-7	27.10	(24)	0.2130	(14)	70.0	1.1	1.08	3.97	6.37	10.9	41.5	18.772	(2)	15.58	(4)	39.25	(4)
Fd-10	27.2	(3)	0.1460	(15)	16.5	1.2	1.42	5.58	6.74	13.6	55.3	18.84	(6)	15.64	(6)	39.35	(6)
WL-6	0.912	(10)	0.1334	(6)	6.5	0.5	0.53	1.84	2.46	13.9	50.0	19.017	(22)	15.663	(23)	39.236	(24)
WL-12	6.56	(6)	0.1384	(5)	10.5	0.4	0.65	1.53	4.03	10.5	25.5	18.946	(28)	15.74	(4)	39.42	(6)
WL-12-R	6.45	(4)															
WL-25	202.3	(26)	0.541	(22)	332	18	0.51	1.45	2.04	16.3	47.9	19.224	(4)	15.61	(5)	39.610	(5)
WL-33	5.086	(27)	0.1503	(5)	20.0	0.4	0.34	1.23	1.81	12.1	45.1	18.72	(4)	15.59	(6)	39.09	(5)
SC-2	174.2	(14)	0.177	(24)	41	19	0.84	7.01	3.43	15.9	137.5	19.040	(15)	15.730	(15)	39.554	(16)
RY-8	13.46	(6)	0.205	(7)	63	6	0.73	2.85	4.19	11.3	45.4	18.731	(2)	15.617	(27)	39.432	(25)
JP-4	12.99	(6)	0.1657	(11)	32.3	0.8	0.41	1.43	5.02	5.3	19.0	18.962	(14)	15.652	(2)	39.152	(24)
JP-8	63.2	(19)	0.145	(12)	16	9	0.37	1.46	4.2	5.7	23.1	18.65	(5)	15.62	(5)	39.00	(4)

ZJ-6	71.7	(4)	0.198	(4)	58.2	2.9	1.32	5.72	5.69	15.1	6.74	19.04	(3)	15.61	(5)	39.44	(5)
LZ-1	951.1	(25)	1.14	(4)	813	34	1.34	6.55	5.68								
LZ-20	176.6	(12)	0.463	(15)	270	12	1.03	4.57	2.57	27.3	124.9	20.45	(5)	15.79	(7)	41.44	(8)
LZ-50	22.62	(10)	0.3360	(29)	168.2	2.3	1.25	1.7	3.66	22.4	31.5	19.22	(6)	15.70	(8)	39.93	(9)
LZ-56	0.568	(19)	0.1247	(3)	−0.5	0.3	1.19	2.55	2.22	35.3	78.1	19.47	(3)	15.63	(5)	40.04	(4)
LZ-66	5.521	(27)	0.1236	(10)	−1.4	0.8	0.64	4.46	6.16	6.7	48.3	18.641	(24)	15.618	(3)	39.40	(4)

	$(^{206}Pb/^{204}Pb)_t$	$(^{207}Pb/^{204}Pb)_t$	$(^{208}Pb/^{204}Pb)_t$	Ni	MgO	Mg#	La/Nb
EMS-3	18.218	15.584	38.634	58	4.64	41	1.2
Jd-3	18.875	15.632	39.190	33	4.41	38	1.1
Jd-10	18.322	15.614	38.900	80	4.24	42	1.2
Fd-2	18.276	15.567	38.612	48	4.22	39	1.1
Fd-3	17.786	15.613	37.983	52	4.73	42	1.0
Fd-7	18.331	15.557	38.726	50	4.07	38	1.1
Fd-10	18.292	15.607	38.648	58	4.44	41	1.1
WL-6	18.454	15.634	38.601	120	6.40	57	1.1
WL-12	18.524	15.720	39.093	182	9.17	63	1.1
WL-12-R							
WL-25	18.566	15.576	39.002	76	5.78	46	0.9
WL-33	18.233	15.567	38.516	58	5.06	45	0.6
SC-2	18.397	15.697	37.809	118	8.21	59	1.2
RY-8	18.277	15.594	38.855	53	6.27	49	0.7
JP-4	18.749	15.641	38.911	67	7.61	46	0.7
JP-8	18.420	15.605	38.709	78	6.88	52	0.8
ZJ-6	18.434	15.579	38.588	62	4.57	37	1.1
LZ-1				76	6.90	53	1.2
LZ-20	19.349	15.737	39.854	36	6.14	50	1.3
LZ-50	18.320	15.652	39.535	20	10.54	63	1.4
LZ-56	18.049	15.558	39.047	122	12.52	68	0.9
LZ-66	18.371	15.604	38.785	263	4.83	41	0.9

Errors are reported as two-standard errors, shown in the parentheses. Uncertainties in Re and Os concentrations and thus $^{187}Re/^{188}Os$ ratios include uncertainties in weighing, error magnification from spiking, and errors in isotopic ratio measurement. Initial Os isotopic compositions were calculated using a ^{187}Re decay constant of 1.666×10^{-11} yr^{-1} (Smoliar et al., 1996).
Initial isotopic ratios and γOs (255 Ma), εNd (255 Ma) in this table were calculated using 255 Ma. γOs (255 Ma) values were calculated using the Os isotope evolution curve of the chondritic mantle with the present $^{187}Os/^{188}Os$ of 0.127. All Os and Pb isotopic data are from this study. Nd isotopic and elemental data of samples from Jinding, Longzhoushan and Zhijin, are also from this study, and their Ti/Y, La/Nb and Mg# values were calculated using data in Table 2. Other εNd (255 Ma) values, Ti/Y, La/Nb, Mg#, Ni, and MgO data in this table are from Xiao et al. (2003a,b, 2004) and this study. All U, Th and Pb concentrations in this table were measured by ICP-MS in the Scripps Institution of Oceanography, University of California, San Diego.

Table 2
Major and trace element composition of high-Ti basalts from Jingding, Zhijin and Longzhoushan

Sample	EMS-3	JD-3	JD-10	FD-2	FD-3	FD-7	FD-10	ZJ-6	LZ-1	LZ-20	LZ-50	LZ-56	LZ-66
Site	Jinding of the Emeishan Mountain							Zhijin	Longzhoushan				
SiO_2	50.81	49.07	52.48	51.28	49.22	51.13	50.67	49.78	50.74	51.65	46.51	46.32	49.17
TiO_2	3.70	3.92	3.60	3.71	3.81	3.98	4.04	4.36	3.03	2.26	3.54	2.79	3.98
Al_2O_3	12.97	12.78	13.38	13.38	14.02	12.79	13.08	13.56	13.69	13.46	9.40	9.92	14.33
Fe_2O_3	4.57	5.90	4.38	4.32	3.92	4.14	4.34	15.17	12.31	11.95	12.23	11.74	13.87
FeO	7.70	7.55	6.50	7.70	8.05	8.20	7.50						
MnO	0.15	0.16	0.14	0.23	0.16	0.18	0.16	0.21	0.16	0.17	0.16	0.16	0.18
MgO	4.64	4.41	4.24	4.22	4.73	4.07	4.44	4.57	6.90	6.14	10.54	12.52	4.83
CaO	8.02	9.19	8.91	7.07	9.19	9.52	8.78	8.68	8.85	9.83	12.28	10.65	9.20
Na_2O	1.89	3.31	1.91	2.86	1.81	1.76	1.99	2.08	1.69	1.88	1.21	0.89	2.26
K_2O	2.04	0.60	1.71	1.86	1.25	1.26	1.33	1.44	1.78	0.90	1.40	1.36	1.04
P_2O_5	0.36	0.34	0.34	0.33	0.35	0.40	0.36	0.42	0.28	0.22	0.30	0.22	0.37
LOI	2.89	2.53	2.13	2.76	3.23	2.32	2.90	0.93	2.32	1.00	2.11	2.81	0.66
SUM	99.74	99.76	99.72	99.72	99.74	99.75	99.59	100.27	101.74	99.45	99.69	99.37	99.87
Cr	73	35	107	61	51	54	79	59	104	113	191	619	1071
Ni	58	33	80	48	52	50	58	62	76	36	20	122	263
Co	37	34	33	35	38	37	37	46	45	44	41	52	58
Sc	23	26	23	28	25	24	25	44	45	46	50	70	55
V	342	349	331	345	363	376	379	473	395	291	255	364	330
Rb	65.8	15.8	57.7	72	39.3	31.9	33.7	36.5	34.8	45.9	33.1	36.5	29.2
Ba	486	266	546	496	530	494	940	576	474	480	370	529	559
Sr	407	564	543	672	539	497	508	555	655	475	381	473	319
Ta	2.5	2.3	2.6	2.5	2.6	2.6	2.7	2.7	2.5	1.7	1.2	2.9	2.6
Nb	36.0	34.0	37.6	36.5	37.9	38.7	38.5	38.3	35.1	25.9	19.8	41.5	36.6
Hf	8.4	8.4	8.9	8.7	8.6	8.9	8.9	9.4	8.8	6.2	5.0	8.4	5.1
Zr	348	356	364	362	359	375	370	341	319	244	194	292	196
Y	32	33	33	32	32	33	31	39	34	30	30	24	18
Th	6.1	5.3	6.1	5.4	7.3	4	5.6	5.7	6.6	4.6	1.7	2.6	4.5
U	1.4	1.3	1.4	1	1.6	1.1	1.4	1.3	1.3	1.0	1.3	1.2	0.6
Pb	7.3	6.6	7.1	6.5	7.4	6.4	6.7	5.7	5.7	2.6	3.7	2.2	6.2
La	42.25	35.85	43.34	39.08	39.01	42.31	40.75	42.09	43.34	33.69	28.09	36.86	33.68
Ce	93.91	84.08	98.08	86.39	90.35	95.2	91.84	94.76	95.67	73.99	60.71	87.02	72.98
Pr	12.48	11.63	12.87	11.64	12.31	12.91	12.31	13.13	12.94	9.69	7.93	12.38	9.52
Nd	51.56	49.73	54.42	48	50.86	54.58	51.92	55.64	54.19	39.30	32.62	54.28	38.60
Sm	10.07	10.02	10.56	9.61	10.08	10.79	10.4	10.94	10.36	8.06	6.87	9.96	6.94
Eu	2.88	2.91	2.98	2.83	2.85	3.1	3.02	3.42	3.07	2.25	2.01	2.93	2.01
Gd	8.28	8.49	8.72	7.96	8.32	9.01	8.77	10.09	9.12	7.41	6.63	7.24	5.68
Tb	1.34	1.38	1.39	1.29	1.35	1.41	1.36	1.46	1.31	1.06	0.99	1.07	0.80
Dy	6.95	7.15	7.23	6.82	6.97	7.17	6.88	8.00	6.92	5.69	5.60	5.30	4.06
Ho	1.26	1.3	1.3	1.23	1.24	1.29	1.25	1.45	1.28	1.04	1.01	0.91	0.72
Er	3.19	3.24	3.3	3.19	3.24	3.24	3.14	3.87	3.37	2.70	2.73	2.33	1.87
Tm	0.46	0.47	0.46	0.46	0.46	0.46	0.46	0.56	0.48	0.38	0.39	0.32	0.28
Yb	2.74	2.83	2.84	2.84	2.75	2.74	2.66	3.22	2.71	2.18	2.37	1.85	1.54
Lu	0.41	0.44	0.43	0.43	0.41	0.42	0.41	0.46	0.39	0.33	0.35	0.26	0.21

Note: Major elements of Jinding samples were analyzed by wet chemistry; major elements of Zhijin and Longzhoushan samples were measured by XRF, their total irons are reported as Fe_2O_3.

In primitive-mantle normalized trace element diagrams (Fig. 2c and d), the high-Ti basalts also have more enriched incompatible element patterns than the low-Ti basalts. In addition, the Emeishan high-Ti basalt samples in this study show a large variation in trace element composition similar to those described by Xu et al. (2001). For example, Jinding high-Ti basalts have incompatible element characteristics similar to OIBs and to HT1-type lavas of the Emeishan CFB province (as defined by Xu et al., 2001), and some of Longzhoushan high-Ti basalts exhibit conspicuous depletions in Th (Fig. 2d) similar to HT2-type lavas (Xu et al., 2001). Also, high-Ti basalts as a whole show a wide range in La/Nb ratios from 0.75 to 1.45, including samples with no Nb anomalies and others with obvious depletions in Nb (Fig. 2c and d), implying that the high-Ti basalts were most likely derived from a rather heterogeneous mantle source.

The Re–Os isotopic data and age-corrected Os isotopic ratios of the Emeishan basalts studied here are listed in Table 1. Sample WL-12 displays good reproducibility for Re and Os concentrations and $^{187}Os/^{188}Os$ ratio in duplicate analyses (Table 1). As a whole, the 21 basalts show variations of Os and Re concentrations, ranging from 3.9 to 559.5 ppt and 31 to 476 ppt, respectively (Table 1). Os

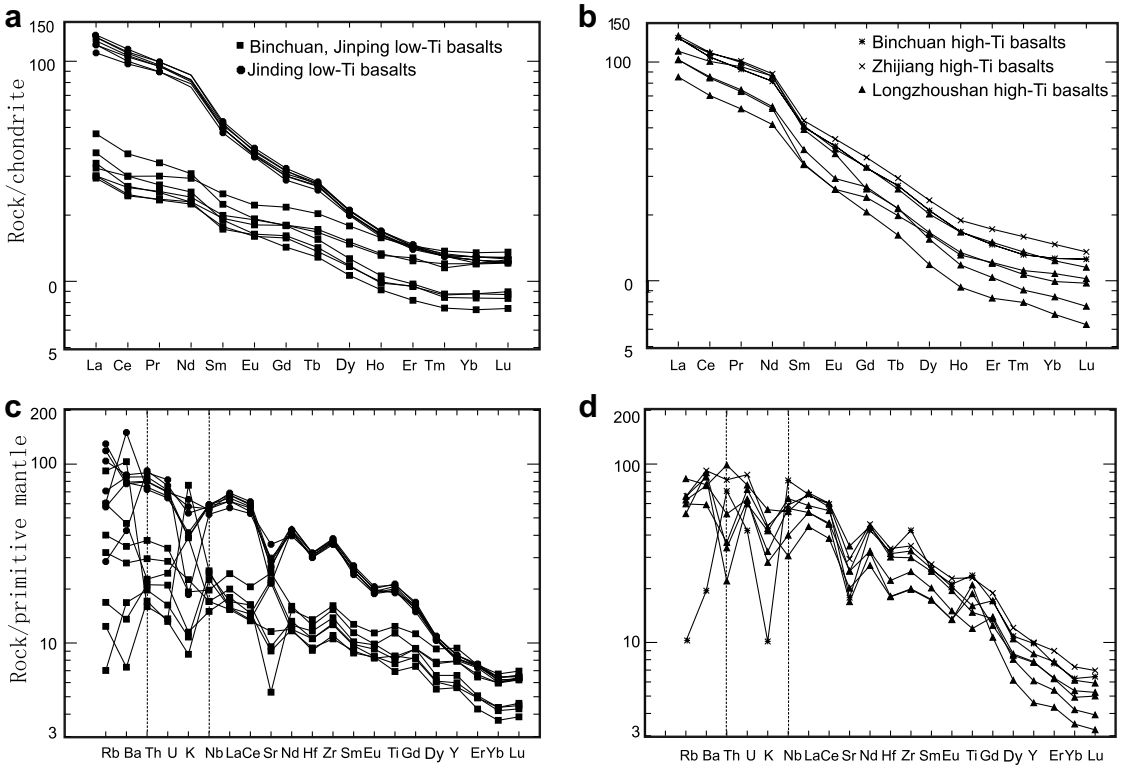

Fig. 2. REE and trace element patterns of Emeishan high and low-Ti basalts from this study. Data for the Binchuan and Jinping basalts are from Xiao et al. (2003a, 2004). Normalizing values for chondrite and primitive mantle are after Sun and McDonough (1989).

concentrations of both high-Ti and low-Ti basalts together display a weak positive correlation with Ni, but Re concentrations do not seem to systematically vary with Ni (not shown). Initial Os isotopic ratios of the Emeishan basalts from different sites span a large range with $(^{187}Os/^{188}Os)_t = 0.1236–1.1455$ and $\gamma Os(t) = -1.4$ to $+813$ (Table 1). $\gamma Os(t)$ values were calculated using the Os evolution curve of the chondritic mantle with the present $^{187}Os/^{188}Os$ of 0.127. The Os isotopic ratios do not show a systematic variation between sites (Fig. 3).

The age-corrected Pb isotopic ratios of Emeishan basalts in this study have a limited variation, with $(^{206}Pb\ ^{204}Pb)_t$ values that vary from 17.786 to 18.875 except for one sample with a $(^{206}Pb\ ^{204}Pb)_t$ greater than 19 (Table 1). This range in Pb isotopic values is similar to plume-related basalts from Hawaii (Lassiter and Hauri, 1998). No significant difference in age-corrected Pb isotopic ratios can be detected between the high-Ti and low-Ti basalt groups. On the other hand, Nd isotopic data analyzed here and Nd and Sr isotopic data reported previously (Xiao et al., 2003b) do show a compositional difference between the high-Ti and low-Ti basalts, i.e., the low-Ti basalts have generally lower $\varepsilon_{Nd}(t)$ and higher initial $^{87}Sr/^{86}Sr$ ratios than the high-Ti basalts (Xiao et al., 2003b). Osmium isotopic compositions of the Emeishan CFBs as a whole do not correlate with variations in Nd, Sr or Pb isotopic compositions (e.g., Fig. 3f). This is similar to igneous rocks from the Gorgona and Curacao island LIP, but distinct from OIBs that have been observed to show good correlations between Os and Nd, Pb and Sr isotopic compositions (Hauri and Hart, 1993; Reisberg et al., 1993; Lassiter and Hauri, 1998; Widom et al., 1999). Therefore, the processes that produced the Emeishan CFBs apparently resulted in a decoupling of Os isotopic composition from the Pb, Nd and Sr isotopic systems (e.g., Walker et al., 1999).

5. DISCUSSION

5.1. Assimilation of shallow-level crustal materials and AFC modeling

Previous studies have considered the possibility of assimilation of crustal materials in the generation of the Emeishan basalts in terms of elemental and Nd and Sr isotopic composition variations (Xiao et al., 2003b; Xu et al., 2001). Our Re–Os isotopic data further confirm that crustal materials were involved in the formation of some Emeishan basaltic magmas through crustal contamination. The $\gamma Os(t)$ values of Emeishan basalts exhibit a complex relationship with Os concentration (Fig. 4) but in general, samples with extremely high $\gamma Os(t)$ have low Os concentrations. Some researchers (e.g., Reisberg et al., 1993; Widom, 1997) have suggested that samples with low Os concentration and anomalously high $^{187}Os/^{188}Os$ ratios most probably experienced assimilation of crustal materials that generally have high Re/Os ratios and thus evolve to very radiogenic Os isotope ratios. For the Emeishan basalts, such samples, which include both low-Ti and high-Ti rocks, possess $(^{187}Os/^{188}Os) > 0.15$. Such high Os isotopic ratios have been observed in some other CFBs (published initial $^{187}Os/^{188}Os$

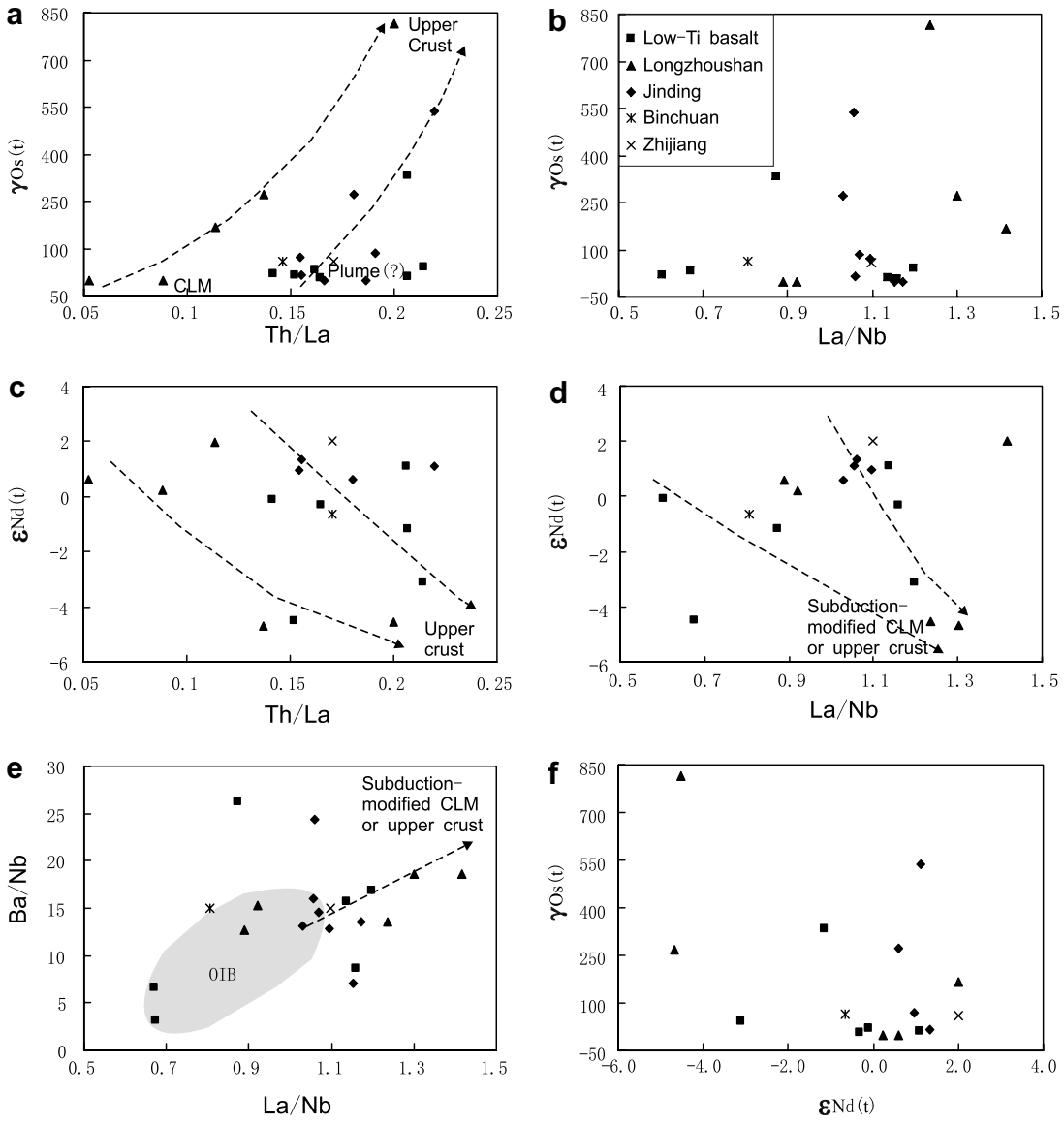

Fig. 3. (a) Th/La vs. γOs(*t*); (b) La/Nb vs. γOs(*t*); (c) Th/La vs. εNd (*t*); (d) La/Nb vs. εNd (*t*); (e) La/Nb vs. Ba/Nb; (f) εNd (*t*) vs. γOs(*t*) diagrams for Emeishan CFBs. Elemental and isotopic data for the Binchuan and Jinping basalts are from Xiao et al. (2003a, 2004). The OIB field is after Sun and McDonough (1989) and Weaver (1991). Subduction-modified continental lithospheric mantle or upper crust is after Xu et al. (2001). Low-Ti basalts shown in the figure are from Binchuan and Jinping sites, the others are high-Ti basalts.

ratios of CFB samples range from 0.1240 to 3.06, Horan et al., 1995; Molzahn et al., 1996; Chesley and Ruiz, 1998) and are also found in modern OIBs such as the Azores and French Polynesia (e.g., 0.1230–0.6138, Widom and Shirey, 1996; Widom, 1997; Shirey and Walker, 1998; Widom et al., 1999). We consider that CFBs with anomalously high initial $^{187}Os/^{188}Os$ ratios were contaminated by shallow-level crustal materials during magma ascent. In the case of Emeishan basalts, the high and low-Ti basalt groups each have distinct trends in Os concentration vs. isotopic composition space (Fig. 4). Except for those with extremely high γOs(*t*), the Emeishan samples yield a relatively narrow range in γOs(*t*) despite a relatively wide range in Os concentration. Therefore, we suggest that the Emeishan basalts JD-3, FD-2, FD-3, FD-7, RY-8, ZJ-6, LZ-1, LZ-20 and LZ-50 among the high-Ti group and WL-25, SC-2, JP-4 and JP-8 among the low-Ti group, were probably contaminated by crustal materials, resulting in anomalously high γOs(*t*) values (Fig. 4 and Table 1). It should be noted that sample FD-10 with a relatively high Os concentration of 68 ppt, has a high $^{187}Os/^{188}Os$ value of 0.1460. However, we do not regard this data point as free of contamination because the γOs(*t*) of FD-10 is significantly higher than those of the other high Os samples in the high-Ti basalt group. Consequently, most of the samples with Os concentrations less than 50 ppt, as well as sample FD-10 with a slightly higher concentration, appear to have been affected by crustal contamination. The Os isotopic composition of

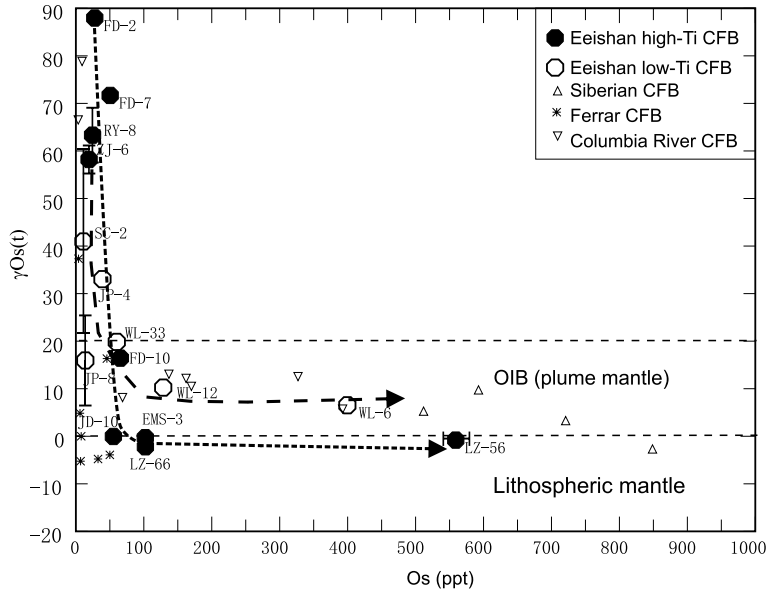

Fig. 4. Os (ppt) vs $\gamma Os(t)$ for the Emeishan CFBs. The Emeishan basalt data plot along two distinct compositional trends (black arrows): low-Ti basalts with radiogenic Os isotopic compositions fall within the OIB (plume mantle) field, while high-Ti basalts have unradiogenic Os isotopic compositions similar to those of SCLM. Samples with $\gamma Os(t) > +90$ are not plotted in this figure for clarity. Data for other CFBs are shown for comparison. OIBs (plume mantle) and lithospheric mantle data ranges are from Shirey and Walker (1998), Widom and Shirey (1996) and Widom et al. (1999). Data sources of other CFBs: Siberian CFBs, Horan et al. (1995); Ferrar CFB, Molzahn et al. (1996) and Riley et al. (2003); Columbia River CFBs, Chesley and Ruiz (1998). Error bars are shown for samples where the uncertainties exceed the size of the symbol.

these contaminated samples cannot represent that of their initial magmas and sources, and their Os isotopic data will not be considered further in the discussion on the mantle source of the Emeishan CFBs.

Plots between Os, Nd isotopes and trace elemental ratios also reveal the presence of crustal contamination in Emeishan CFBs. Compositional variation trends toward the upper crust can been seen in Fig. 3a and c. For example, samples from the Longzhoushan and Jinding sites clearly show a variation from low to high $\gamma Os(t)$ and Th/La ratios with addition of upper crustal material, confirming that crustal assimilation did indeed modify Os isotopic and elemental compositions of some Emeishan CFBs.

We need to evaluate whether the samples with higher Os concentrations (>50 ppt) have experienced any significant crustal contamination affecting their $\gamma Os(t)$ values. Neither the high nor low Os concentration groups show any correlation between Os and Nd isotope compositions (Fig. 3f). Specifically, the low Os concentration samples do not have lower $\varepsilon_{Nd}(t)$ or higher initial $^{87}Sr/^{86}Sr$ values (data after Xiao et al., 2003a,b, 2004) than those with high Os concentrations. This implies that Nd and Sr isotopic compositions are less sensitive to crustal contamination than Os isotopes (Chesley and Ruiz, 1998). Nonetheless, the possibility that the high Os concentration samples were also contaminated with crust cannot be ignored. However, because shallow crustal materials generally have very low Os contents (Peucker-Ehrenbrink and Jahn, 2001; Hattori et al., 2003), the radiogenic Os isotopic compositions of lavas with relatively high Os concentrations (>50 ppt and $\gamma Os(t) > +10$, i.e., WL-6, WL-12) are not easily explained by crustal contamination (Becker, 2000). The Emeishan basalts with high Os contents therefore most likely experienced very little or no crustal contamination, and we believe that their age-corrected Os isotopic compositions may reflect the isotopic characteristics of their initial magmas and mantle sources. In summary, crustal assimilation clearly affected the Re–Os isotopic composition of some but not all of the Emeishan samples, and the basalts with high Os concentration are the least-contaminated samples.

Assuming the least-contaminated sample, WL-6, as representative of the parental magma of the low-Ti basalts, and EMS-3 or LZ-56 as parental magmas of the high-Ti basalts, we have modeled the Os isotope variation of Emeishan basalts based on a simple mixing and an assimilation fractional crystallization (AFC) model (DePaolo, 1981). It is assumed in the AFC modeling that the Emeishan basaltic magmas experienced assimilation of continental crust and crystal fractionation of an olivine + sulphide assemblage with differing olivine–sulphide proportions. Fig. 5 shows that simple mixing cannot reproduce the Os isotopic trends of both high and low-Ti basalts. On the other hand, if the parental magmas represented by the least-contaminated samples experienced AFC processes, modeling results are consistent with observed variations in Os isotope compositions. In addition, the calculations also indicate that ~3% to 5% of upper crust materials were assimilated by the Emeishan magmas during crystal fractionation. These modeling results demonstrate that assimilation of crustal material can produce the Os isotopic signatures of the differentiated members of both Emeishan high-Ti and low-Ti basalts. However, the higher $^{187}Os/^{188}Os$ ratios of Os rich low-Ti basalts cannot result from AFC contamination of high-Ti magmas.

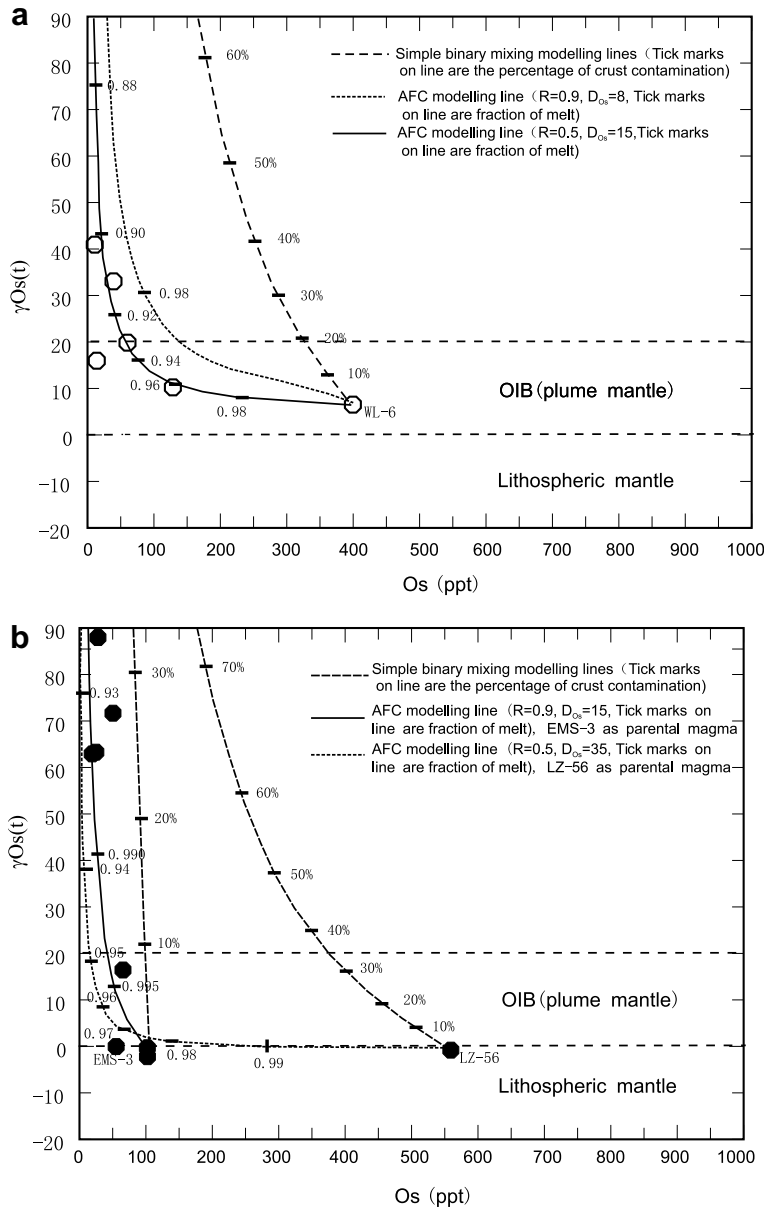

Fig. 5. AFC (assimilation fractional crystallization) and simple mixing modeling for Emeishan high and low-Ti basalts using presumed Emeishan parental magmas and average continental crust: (a) low-Ti basalt, using WL-6 as the starting composition for the parental magma, (b) high-Ti basalts, taking EMS-3 and LZ-56 as parental magma starting compositions. Average continental crust values used are [Os] = 30 ppt, γOs(0 Ma) = 860 and, γOs(255 Ma) = 740 (after Peucker-Ehrenbrink and Jahn, 2001; Hattori et al., 2003). The parameters used for the AFC modeling are: R [(rate of assimilation of crust)/(rate of fractional crystallization)], D_{Os} is the bulk solid/liquid partition coefficient for Os, which is calculated for olivine + sulphide fractionation assuming $K_{d\ Os}$ olivine/melt = 7 (between olivine and melt), $K_{d\ Os}$ sulphide/melt = 15,000 (between sulphide and melt) (after McBride et al., 2001) using different percentages of olivine and sulphide fractionation. Both diagrams show that a simple mixing model cannot reproduce the compositional trend of both high and low-Ti basalts, whereas, if the parental magmas experienced AFC processes, modeling results are consistent with the observed Os isotopic variation of the Emeishan samples.

5.2. Genesis of high-Ti and low-Ti basalts

High-Ti and low-Ti basalts are generally the dominant lava types in continental flood basalt provinces, e.g., Ferrar (Molzahn et al., 1996), Columbia River (Chesley and Ruiz, 1998), and Emeishan (Xu et al., 2001). In the case of the Emeishan CFB, the low-Ti basalts erupted earlier than the high-Ti basalts, as they occur in the lower section in the southwest part of the province (Binchuan), whereas the high-Ti basalts are distributed in the upper section in the Binchuan area, and in the center, east and north (Fig. 1). The two compositions have distinct elemental and Nd–Sr isotopic features (Fig. 2 and Xiao et al., 2003b), suggesting that they were derived from distinct sources or have experienced different petrogenetic processes. However, the genetic relationship between the

high-Ti and low-Ti basalts, and their magmatic sources, are still disputed. Xu et al. (2001) proposed that the thick low-Ti lavas in the western part may record the main episode of flood basalt emplacement, whereas the overlying high-Ti basalts represent the waning activity of the plume and were products of lower degrees of mantle melting beneath relatively thicker lithosphere with a lower geotherm. However, Xiao et al. (2004) argued that the low-Ti basaltic magmas may have assimilated crustal material and that the metasomatized subcontinental lithospheric mantle may have been the major source for their generation, whereas the high-Ti lavas may have been derived from the plume mantle directly, with little contamination by crustal material.

We note that the high-Ti basalts from the Emeishan LIP have an Os isotopic composition signature distinct from that of the low-Ti basalts. If the samples with extremely high $\gamma Os(t)$ ($> +50$) and low Os concentrations are excluded (Fig. 4), the Emeishan high-Ti and low-Ti basalts, have compositions that plot on two distinct trends: low-Ti basalts have radiogenic Os isotopic composition similar to that of plume-related OIBs, whereas the high-Ti basalts show unradiogenic Os isotopic features similar to that of SCLM. Considering that the low-Ti basalts were erupted slightly earlier than the high Ti-basalts in the southwest part of the Emeishan LIP (e.g., Binchuan area), the question arises as to whether the high-Ti basalts were produced by partial melting of the same mantle from which the low-Ti basaltic melts had been extracted. This possibility may be ruled out because earlier erupted melts are generally expected to contain more enriched incompatible elements than later erupted melts from the same mantle source. Instead, the high-Ti basalts have higher incompatible element contents than the low-Ti basalts, indicating a more enriched source rather than a depleted source. In addition, Xiao et al. (2004) and Xu et al. (2001) also concluded on the basis of elemental and isotopic data that the chemical variation between high and low-Ti basalts cannot be described by simple crystal fractionation from a common parental magma. Thus, we consider that the primary melts of the low and high-Ti basalts originated from two distinct mantle sources.

5.2.1. Evidence for a mantle plume origin

It has previously been suggested from the Re–Os isotopic compositions of high-Mg volcanic rocks of the Karoo and Siberian CFBs that they were mainly derived from a mantle plume (Ellam et al., 1992; Horan et al., 1995). Plume-derived OIBs with high Os contents have relatively radiogenic Os signatures, with limited variation, which have been regarded as representing the Os isotopic signature of their respective mantle plume sources (Hauri and Hart, 1993; Reisberg et al., 1993; Walker et al., 1995; Widom and Shirey, 1996; Widom et al., 1999; Eisele et al., 2002). In the case of the Emeishan CFBs, the low-Ti basalts with the highest Os concentation (e.g., WL-6), and which probably experienced the least crustal contamination according to its Os isotopic composition, most likely reflects the Os isotopic composition of the low-Ti basalt mantle source. As shown in Fig. 4, sample WL-6 has a radiogenic Os isotopic composition ($\gamma Os(t) = +6.5$), which is within the range attributed to mantle plumes (Widom and Shirey, 1996; Widom et al., 1999).

It should be noted that Emeishan low-Ti basalts have variable La/Nb ratios (Fig. 2c and Table 1). A number of low-Ti lavas have La/Nb ratios greater than 1, which differs from the values of typical plume-derived OIBs. Xiao et al. (2004) suggested that the lavas with relatively high La/Nb ratios (LT1 type) contain a significant contribution from continental lithospheric mantle. However, as shown in Fig. 2c, most of the low-Ti basalts display no negative Nb anomaly, and especially, samples with a plume signature such as WL-6 and WL-12, have La/Nb ratios close to 1. Therefore, we suggest that at least sample WL-6 and WL-12 most likely contain little lithospheric component. On the other hand, those samples with relatively high La/Nb ratios also have generally high $^{187}Os/^{188}Os$ ratios and $\gamma Os(t)$ values, suggesting that their magmas were probably contaminated by a lower crustal materials, thus producing relatively high La/Nb ratios in the low-Ti samples.

The $\varepsilon_{Nd}(t)$ vs. $\gamma Os(t)$ and ($^{206}Pb^{204}Pb$) vs. $\gamma Os(t)$ (Fig. 6) diagrams further support the suggestion that the low-Ti basalts most likely have a genetic link to a mantle plume. In Fig. 6a, the data for the Emeishan low-Ti basalt samples with high Os concentration display a narrow $\varepsilon_{Nd}(t)$ range relative to OIBs and other CFBs, but plot within the field of OIBs, suggesting that plume material likely made a significant contribution to the generation of the low-Ti basaltic melts. In the Pb–Os isotope diagram (Fig. 6b), the low-Ti basalt WL-6 also plots in the field of typical enriched plume end member (EP) defined by Shirey and Walker (1998). In summary, the Emeishan low-Ti basalts, as typified by samples WL-6 and WL-12, are most likely melting products of a mantle plume.

5.2.2. Contribution of a lithospheric mantle component

Re–Os isotopic compositions of the dominantly basaltic lavas from large igneous provinces (LIPs) suggest that a subcontinental lithospheric mantle (SCLM) source was not significantly involved in the formation of the Columbia River CFBs (Chesley and Ruiz, 1998), whereas an enriched SCLM component played an important role in the production of the Ferrar CFBs (Molzahn et al., 1996). In contrast to the low-Ti basalt samples with high Os concentrations, the four Emeishan high-Ti basalt samples (EMS-3; JD-10, LZ-56, LZ-66) have a limited range of unradiogenic Os isotopic values ($\gamma Os(t) = -1.4$ to -0.8), with relatively high Os concentrations from 55.4 to 559.5 ppt. These four samples have Os isotopic characteristics similar to the unradiogenic OIB group from the Canary Island defined by Widom et al. (1999). Widom et al. (1999) interpreted these to result from a plume-melt that had assimilated lithospheric mantle with negative $\gamma Os(t)$ and $\varepsilon_{Nd}(t)$, resulting in the generation of OIBs with unradiogenic Os isotopic compositions. A similar interpretation was made for the Karoo CFBs on the basis of unradiogenic Os and Nd compositions (Ellam et al., 1992). We propose that the Emeishan high-Ti basalt samples with unradiogenic Os isotopes also have a similar origin, and that their magmas were most likely contaminated by SCLM material. In a $\gamma Os(t)$ vs. $\varepsilon_{Nd}(t)$ diagram (Fig. 6a), data for these Emeishan high-Ti basaltic samples

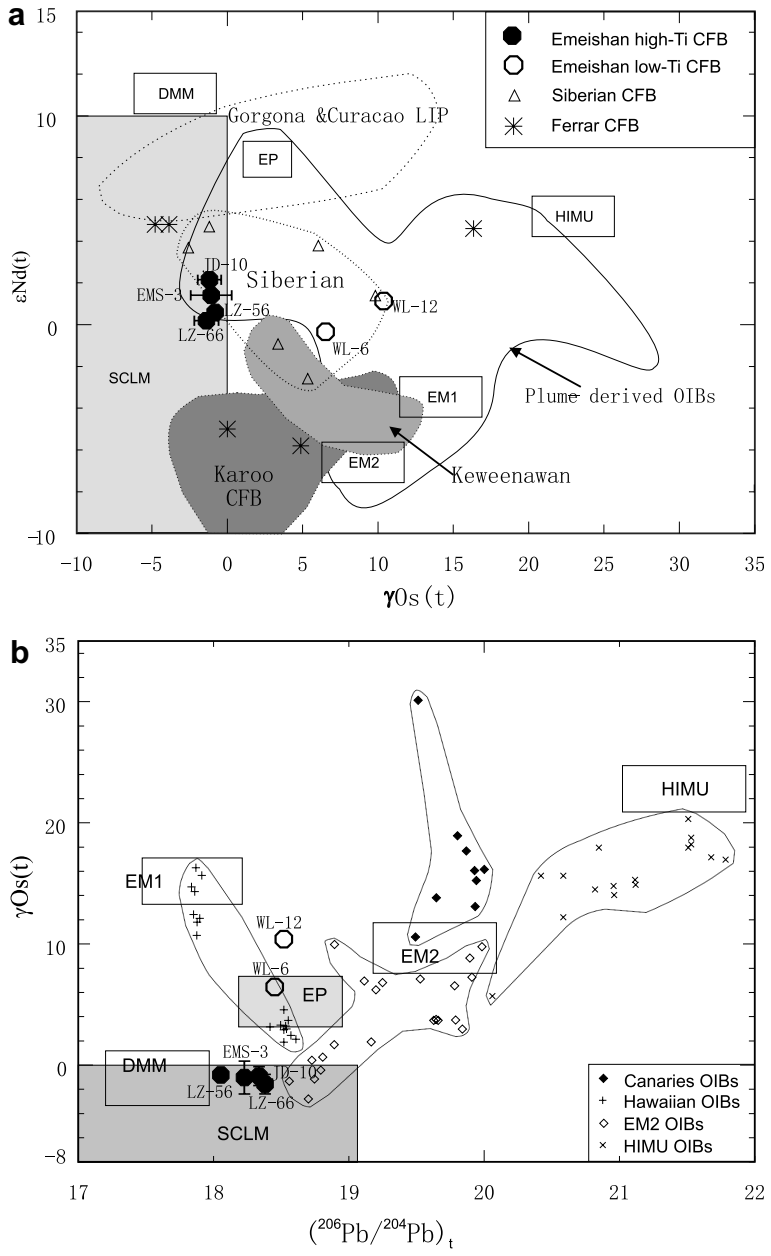

Fig. 6. Plots of (a) $\gamma Os(t)$ (t, eruption time) vs εNd (t) and (b) $(^{206}Pb^{204}Pb)_t$ vs $\gamma Os(t)$ for the Emeishan CFBs. Only data for high- and low-Ti basalts with little or no crustal contamination signature (e.g., LZ-56, LZ-66, JD-10 and EMS-3 for high-Ti and WL-6 and WL-12 for low-Ti basalts) are plotted. In (a) EM1, EM2, HIMU, EP and DMM end members are from Shirey and Walker (1998). SCLM field is after Shirey and Walker (1998) but $\varepsilon_{Nd}(t)$ values may extend to +10 according to new data (Zhang et al., 2000; Handler et al., 2005). Data fields for plume-derived OIBs are modified according to available data (Hauri and Hart, 1993; Reisberg et al., 1993; Marcantonio et al., 1995; Widom and Shirey, 1996; Lassiter and Hauri, 1998; Widom et al., 1999). Data fields for the Karoo and Keweenawan CFBs are from Shirey and Walker (1998) and from Walker et al. (1999) for the Gorgona and Curacao LIPs. Data sources for the Ferrar and Siberian CFBs are as in Fig. 4. The data for the Emeishan low-Ti basaltic samples plot within the plume-melts field, and those of the high-Ti basaltic samples fall in the SCLM field. In (b) crosses represent data for Hawaiian plume-derived OIBs (Lassiter and Hauri, 1998). Other data sources are Marcantonio et al. (1995) for the Canary Islands, Reisberg et al. (1993), Hauri and Hart (1993) and Widom and Shirey (1996) for EM2 and HIMU OIBs, and the SCLM field is constructed by taking $\gamma Os(t) < 0$ (Handler et al., 2005; Shirey and Walker, 1998) and using Pb isotopic data for the lithosphere mantle from Choi et al. (2005). Except where error bars are shown, $\gamma Os(t)$ errors are smaller than the sample symbol size.

and some Siberian LIP lavas plot in the SCLM field. The age of the lithospheric mantle beneath Emeishan CFBs is uncertain but the fact that most lavas are distributed in the Yangtze craton region (Fig. 1) implies that the subcontinental lithosphere mantle is likely rather old. Such old SCLM is expected to have a generally unradiogenic Os isotopic signature similar to that of Karoo and Siberian CFBs, and addition of such material to the source will drive magma compositions to negative γOs values. Thus, we believe that the Emeishan high-Ti basaltic magmas contain a litho-

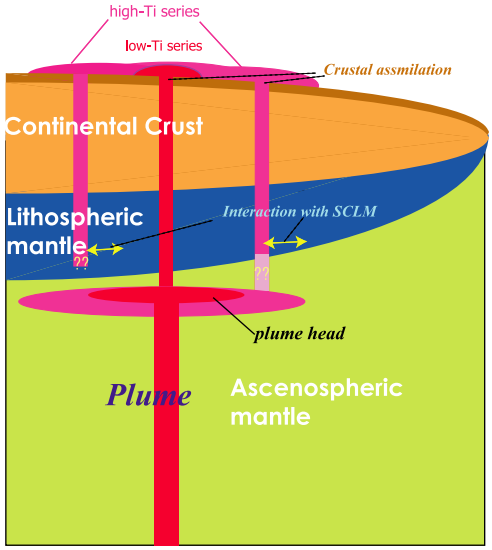

Fig. 7. Model for the origin of the Emeishan high and low-Ti basalts, showing that they were derived from different mantle sources, respectively, and experienced different plume-related magmatic processes.

spheric component. However, the Emeishan high-Ti basalts have $\gamma Os(t)$ and $\varepsilon_{Nd}(t)$ values higher than those of the Karoo CFBs (Fig. 6a), suggesting that they either contain less lithospheric mantle material than the Karoo lavas, or that they assimilated SCLM that was younger or less unradiogenic than the sub-Karoo CLM.

In addition, as mentioned above, the high-Ti basalts in this study have a wide La/Nb ratio range (0.75–1.45, Table 1) and some of them clearly exhibit negative Nb anomalies (Longzhoushan samples, Fig. 2d). Xu et al. (2001) also observed a large variation of La/Nb ratios among their Emeishan high-Ti samples. High La/Nb ratios and clear negative Nb anomalies in the high-Ti basalts strongly support the suggestion that lithospheric mantle components were involved in generation of the high-Ti basalts. La/Nb vs. Ba/Nb and $\varepsilon_{Nd}(t)$ diagrams (Fig. 3d and e) also show that the Emeishan high-Ti basalts in this study display a compositional variation toward subduction-modified continental lithospheric mantle with generally high La/Nb, Ba/Nb ratios and low $\varepsilon_{Nd}(t)$ values. Therefore, Os and Nd isotopic compositions coupled with elemental data reveal the contribution of a lithospheric component to the high-Ti basaltic magmas.

Based on the Os–Nd–Pb isotopic data, two hypotheses may explain the origin and compositional variations of the Emeishan high-Ti basalts. One possibility is that the Emeishan high-Ti basaltic magmas were partial melting products of a SCLM that was heated and uplifted by the underplating (or ascending) mantle plume, thereby producing unradiogenic Os isotopic signatures similar to that of SCLM. Another possibility is that primitive high-Ti basaltic magmas were derived from a different part (shallow level?) of the mantle plume relative to the low-Ti basalts, and then mixed with significant SCLM material during ascent through the SCLM (Fig. 7). The addition of a SCLM component to the primitive plume melts would thus have produced high-Ti basaltic magmas with an unradiogenic Os composition. With the currently available data, it is difficult to distinguish between these possibilities. Xu et al. (2001) concluded that Emeishan high-Ti basalts represented the waning activity of the plume on the basis of Nd and Sr isotopic and elemental geochemistry. Their conclusion is consistent with the second hypothesis. On the other hand, our Os isotopic data do not support the contention of Xiao et al. (2004) that the low-Ti basalt source was derived from the lithospheric mantle. Rather, it is the high-Ti basalts that have Os compositions more indicative of a SCLM contribution. Fig. 7 shows a schematic of the Emeishan mantle plume model and the possible genesis of high and low-Ti basalts.

6. CONCLUSIONS

(1) This study shows that the low-Ti Emeishan CFBs have radiogenic Os signatures similar to plume-derived OIBs, suggesting that the generation of the Emeishan LIP may be attributed to a mantle plume.
(2) The low-Ti basalts from the Emeishan LIP have Os isotope as well as chemical compositions distinct from the high-Ti basalts. The former may have originated from a mantle plume source, whereas the latter were more likely derived from a lithospheric mantle source. Alternatively, the high-Ti basalts may have been derived from a different region of the mantle plume and interacted significantly with lithospheric mantle material en route to the surface.

ACKNOWLEDGMENTS

Xu J.-F. sincerely thanks the JSPS (Japan Society for the Promotion of Science) – CAS (Chinese Academy of Sciences) – cooperative program that funded him to conduct the Re–Os isotopic analyses presented, and the Institute of Geothermal Sciences, Kyoto University for providing access to their Re–Os isotopic laboratory. Special thanks to Dr. P. Castillo who helped us obtain U, Th, and Pb concentration measurements at SIO, UCSD. We are very much indebted to M.L.G. Tejada and Monica Handler for their critical comments on the earlier version of our manuscript. Laurie Reisberg and two anonymous reviewers are thanked for their constructive comments. We thank K. Abe for assistance with Re–Os analyses. This study was financially supported by the National Natural Science Foundation of China (40421303, 40234046; 40425003), Chinese Academy of Sciences (KZCX3-SW-143:4, A15-041107), the Major State Basic Research Program of People's Republic of China (No. 2002CB412602), and a Grant-in-Aid (#14703002) from JSPS (Japan Society for the Promotion of Science).

REFERENCES

Becker H. (2000) Re–Os fractionation in eclogites and blueschists and the implications for recycling of oceanic crust into the mantle. *Earth Planet. Sci. Lett.* **177**, 131–345.

Boven A., Pasteels P., Punsalan L. E., Liu J., Luo X., Zhang W., Guo Z., and Hertogen J. (2002) $^{40}Ar/^{39}Ar$ geochronological

constraints on the age and evolution of the Permo-Triassic Emeishan volcanic province, southwest China. *J. Asian Earth Sci.* **20**, 157–175.

Campbell I. H., and Griffiths R. W. (1990) Implications of mantle plume structure for the evolution of flood basalts. *Earth Planet. Sci. Lett.* **99**, 79–93.

Chesley J. T., and Ruiz J. (1998) Crust–mantle interaction in large igneous provinces: implications from the Re–Os isotope systematics of the Columbia River flood basalts. *Earth Planet. Sci. Lett.* **154**, 1–11.

Choi S. H., Kwon S.-T., Mukasa S. B., and Sagong H. (2005) Sr–Nd–Pb isotope and trace element systematics of mantle xenoliths from Late Cenozoic alkaline lavas. *Chem. Geol.* **221**, 40–64.

Chung S. L., and Jahn B. M. (1995) Plume–lithosphere interaction in generation of the Emeishan flood basalts at the Permian–Triassic boundary. *Geology* **23**, 889–892.

Chung S. L., Jahn B. M., Wu G. Y., Lo C. H., and Cong B. L. (1998) The Emeishan flood basalt in SW China: a mantle plume initiation model and its connection with continental break-up and mass extinction at the Permian–Triassic boundary. In *Mantle Dynamics and Plate Interaction in East Asia AGU Geodyn* (eds. M. F. J. Flower, S. L. Chung, C. H. Lo, T. Y. Lee), Ser. vol. 27, AGU, Washington, DC, pp. 47–58.

Coffin M. F., and Eldholm O. (1994) Large igneous provinces: crustal structure, dimension, and external consequences. *Rev. Geophys.* **32**, 1–36.

Cohen A. S., and Waters G. G. (1996) Separation of osmium from geological materials by solvent extraction for analysis by thermal ionization mass spectrometry. *Anal. Chim. Acta* **332**, 269–275.

Creaser R. A., Papanastassiou D. A., and Wasserburg G. J. (1991) Negative thermal ion mass spectrometry of osmium, rhenium, and iridium, Geochim. *Cosmochim. Acta* **55**, 397–401.

DePaolo D. (1981) Trace element and isotopic effects of combined wallrock assimilation and fractional crystallization. *Earth Planet. Sci. Lett* **53**, 189–202.

Eisele J., Sharma M., Galer S. J. G., Blichert-Toft J., Devey C. W., and Hofmann A. W. (2002) The role of sediment recycling in EM-1 inferred from Os, Pb, Hf, Nd, Sr isotope and trace element systematics of the Pitcairn hotspot. *Earth Planet. Sci. Lett* **196**, 197–212.

Ellam R. M., Carlson R. W., and Shirey S. B. (1992) Evidence from Re–Os isotopes for plume–lithosphere mixing in Karoo flood basalt genesis. *Nature* **359**, 718–721.

Handler M. R., Bennett V. C., and Carlson R. W. (2005) Nd, Sr and Os isotope systematics in young fertile spinel peridotite xenoliths from northern Queensland Australia: a unique view of depleted MORB mantle. *Geochim. Cosmochim. Acta* **69**, 5747–5763.

Hattori Y., Suzuki K., Honda M., and Shimizu H. (2003) Re–Os isotope systematics of the Taklimakan desert sands, moraines and river sediments around the Taklimakan desert, and of Tibetan soils. *Geochim. Cosmochim. Acta* **67**, 1195–1205.

Hauri E. H., and Hart S. R. (1993) Re–Os isotope systematics of HIMU and EMII oceanic island basalts from the south Pacific Ocean. *Earth Planet. Sci. Lett.* **114**, 353–371.

He B., Xu Y. G., Chung S.-L., Xiao L., and Wang Y. M. (2003) Sedimentary evidence for a rapid, kilometer-scale crustal doming prior to the eruption of the Emeishan flood basalts. *Earth Planet. Sci. Lett.* **213**, 391–405.

Horan M. F., Walker R. J., Fedorenko V. A., and Czamanske G. (1995) Osmium and neodymium isotopic constraints on the temporal and spatial evolution of Siberian flood basalt sources. *Geochim. Cosmochim. Acta* **59**, 5159–5168.

Huang K., and Opdyke N. D. (1998) Magnetostratigraphic investigations on an Emeishan basalt section in western Guizhou Province, China. *Earth Planet. Sci. Lett.* **163**, 1–14.

Kamo S. L., Czamanske G. K., Amelin Y., Fedorenko V. A., Davis D. W., and Trofimov V. R. (2003) Rapid eruption of Siberian flood–volcanic rocks and evidence for coincidence with the Permian–Triassic boundary and mass extinction at 251 Ma. *Earth Planet. Sci. Lett.* **214**, 75–91.

Kato Y., Fujinaga K., and Suzuki K. (2005) Major and trace element geochemistry and Os isotopic composition of metalliferous umbers from the late Cretaceous Japanese accretionary complex. *Geochemsitry Geophysics Geosystem* **6**, Q07004. doi:10.1029/2005GC00092.

Lassiter J. C., and Hauri E. H. (1998) Osmium-isotope variations in Hawaiian lavas: evidence for recycled oceanic lithosphere in the Hawaiian plume. *Earth Planet Sci. Lett.* **164**, 483–496.

Li X.-H. (1997) Geochemistry of the Longsheng ophiolite from the southern margin of Yangtze craton, SE China. *Geochem. Jour.* **31**, 323–337.

Liang X. R., Wei G. J., Li X. H., and Liu Y. (2003) Precise determination of $^{143}Nd/^{144}Nd$ and Sm/Nd ratios using multiple-collector inductively coupled plasmamass spectrometer (MC-ICPMS). *Geochimica* **32**, 91–96, in Chinese with Eanglish abstract.

Lin J. Y. (1985) Spatial and temporal distribution of Emeishan basaltic rocks in the three southwestern provinces (Sichuan, Yunnan and Guizhou) of China. *China. Bull. Sci.* **12**, 929–932.

Lo C. H., Chung S. L., Lee T. Y., and Wu G. Y. (2002) Age of the Emeishan flood magmatism and relations to Permian–Triassic boundary events. *Earth Planet. Sci. Lett.* **198**, 449–458.

McBride J. S., Lambert D. D., Nicholls I. A., and Price R. C. (2001) Osmium isotopic evidence for crust–mantle interaction in the genesis of continental intraplate basalts from the Newer volcanics province, Southeastern Australia. *J. Petrol.* **42**, 1197–1218.

Marcantonio F., Zindler A., Elliott T., and Staudigel H. (1995) Os isotope systematics of La Palma, Canary Islands: evidence for recycled crust in the mantle source of HIMU ocean islands. *Earth Planet. Sci. Lett.* **133**, 397–410.

Meisel T., Walker R. J., Irving A. J., and Lorand J.-P. (2001) Osmium isotopic compositions of mantle xenoliths: a global perspective. *Geochim. Cosmochim. Acta* **65**, 1311–1323.

Molzahn M., Reisberg L., and Wörner G. (1996) Os, Sr, Nd, Pb, O isotope and trace element data from the Ferrar flood basalts, Antarctica: evidence for an enriched subcontinental lithospheric source. *Earth Planet. Sci. Lett.* **144**, 529–546.

Nier A. O. (1950) A redetermination of the relative abundances of the isotopes of carbon, nitrogen, oxygen, argon and potassium. *Phys. Rev. B* **77**, 789–793.

Pearson D. G., and Woodland S. J. (2000) Solvent extraction/anion exchange separation and determination of PGEs (Os, Ir, Pt, Pd, Ru) and Re–Os isotopes in geological samples by isotope dilution ICP-MS. *Chem. Geol.* **165**, 57–107.

Peucker-Ehrenbrink B., and Jahn B. (2001) Rhenium–osmium isotope systematics and platinum group element concentrations: loess and the upper continental crust. *Geochem. Geophys. Geosyst.* **2**(10). doi:10.1029/2001GC00017.

Reisberg L., Zindler A., Marcantonio F., White W., Wyman D., and Weaver B. (1993) Os isotope systematics in ocean island basalts. *Earth Planet. Sci. Lett.* **129**, 149–167.

Renne P. R., Zhang Z. C., Richards M. A., Black M. T., and Basu A. R. (1995) Synchrony and causal relations between Permian–Triassic boundary crises and Siberian flood volcanism. *Science* **269**, 1413–1416.

Riley T. R., Leat P. T., Storey B. C., Parkinson I. J., and Millar I. (2003) Ultramafic lamprophyres of the Ferrar large igneous

province: evidence for a HIMU mantle component. *Lithos* **66**, 63–76.

Roy-Barman, M. (1993) Mesure du rapport $^{187}Os/^{188}Os$ dans les basaltes et les peridotites: contribution a la systematique ^{187}Re–^{187}Os dans le manteau, Ph.D. Thesis, Universite de Paris VII.

Shirey S. B., and Walker R. J. (1995) Carius tube digestion for low-blank rhenium–osmium analysis. *Anal. Chem.* **67**, 2136–2141.

Shirey S. B., and Walker R. J. (1998) The Re–Os isotope system in cosmochemistry and high-temperature geochemistry. *Annu. Rev. Earth Planet. Sci.* **26**, 423–500.

Smoliar M. I., Walker R. J., and Morgan J. W. (1996) Re–Os ages of group IIA, IIIA, IVA and IVB iron meteorites. *Science* **271**, 1099–1102.

Sun S.-S., and McDonough W. F. (1989) Chemical and isotopic systematics of ocean basalts: implications for mantle composition and processes. In *Magmatism in the Ocean Basins* (eds. A.D. Saunders and M.J. Norry). Blackwell Scientific, London, pp. 313–345.

Suzuki K., and Honda M. (2003) *Analytical Method of Osmium and Rhenium Isotopes. Frontire Research on Earth Evolution*, vol. 1, IFREE REPORT for 2001–2002, pp. 379–381.

Suzuki K., Miyata Y., and Kanazawa N. (2004) Precise Re isotope ratio measurements by negative thermal ionization mass spectrometry (NTI-MS) using total evaporation technique. *Int. J. Mass Spectrom.* **235**, 97–101.

Volkening J., Walczyk T., and Heumann K. G. (1991) Osmium isotope ratio determinations by negative thermal ionization mass spectrometry. *Int. J. Mass Spectrom. Ion Process.* **105**, 147–159.

Walker R. J., Morgan J. W., and Horan M. F. (1995) ^{187}Os enrichment in some mantle plume source: evidence for core-mantle interaction? *Science* **269**, 819–822.

Walker R. J., Storey M., Kerr A. C., Tarney J., and Arndt N. T. (1999) Implications of ^{187}Os isotopic heterogeneities in a mantle plume: evidence from Gorgona Island and Curaçao. *Geochim. Cosmochimi. Acta* **63**, 713–728.

Weaver B. L. (1991) The origin of ocean island basalts end-member composition: trace element and isotopic constraints. *Earth Planet. Sci. Lett.* **104**, 381–397.

Widom E. (1997) Sources of ocean island basalts: a review of the osmium isotope evidence. *Phys. A.* **244**, 484–496.

Widom E., and Shirey S. B. (1996) Os isotope systematics in the Azores: implications for mantle plume sources. *Earth Planet. Sci. Lett.* **142**, 451–465.

Widom E., Hoernle K. A., Shirey S. B., and Schmingcke H.-U. (1999) Os isotope systematics in the Canary Ialands and Madeira: lithospheric contamination and mantle plume signatures. *J. Petrol.* **40**, 279–296.

Wei G. J., Liang X. R., Li X. H., and Liu Y. (2002) Precise measurement of Sr isotopic composition of liquid and solid base suing (LP) MC-ICPMS. *Geochimica* **31**, 35–42, in Chinese with Eanglish abstract.

Xiao L., Xu Y.-G., Chung S.-L., He B., and Mei H.-J. (2003a) Chemostratigraphic correlation of upper permian lavas from Yunnan Province, China: extent of the Emeishan large igneous province. *Intern. Geol. Rev.* **45**, 754–766.

Xiao L., Xu Y.-G., and He B. (2003b) Emei mantle plume-subcontinental lithosphere interaction: Sr–Nd and O isotopic evidences from low-Ti and high-Ti basalts. *Geol. J. China Univ.* **9**, 207–217.

Xiao L., Xu Y.-G., Mei H.-J., and He B. (2003c) Late Permian flood basalts at Jinping area and its relation to Emei mantle plume: geochemical evidences. *Acta Petrol. Sin.* **19**, 38–48.

Xiao L., Xu Y. G., Mei H. J., Zheng Y. F., He B., and Pirajno F. (2004) Distinct mantle sources of low-Ti and high-Ti basalts from the western Emeishan large igneous province, SW China: implications for plume–lithosphere interaction. *Earth Planet. Sci. Lett.* **228**, 525–546.

Xu J.-F., Castillo P. R., Li X.-H., Yu X.-Y., Zhang B.-R., and Han Y.-W. (2002) MORB-type rocks from the Paleo-Tethyan Mian-Lueyang northern ophiolite in the Qinling Mountains, central China: implications for the source of the low $^{206}Pb/^{204}Pb$ and high $^{143}Nd/^{144}Nd$ mantle component in the Indian ocean. *Earth Planet. Sci. Lett.* **198**, 323–337.

Xu Y. G., Chung S. L., Jahn B. M., and Wu G. Y. (2001) Petrologic and geochemical constraints on the petrogenesis of Permian–Triassic Emeishan flood basalts in SW China. *Lithos* **58**, 145–168.

Xu Y.-G., He B., Chung S. L., Menzies M. A., and Frey F. A. (2004) The geologic, geochemical and geophysical consequences of plume involvement in the Emeishan flood basalt province. *Geology* **30**, 917–920.

Zhang M., Suddaby P., O'Reilly S. Y., Norman M., and Qi J. X. (2000) Nature of the lithospheric mantle beneath the eastern part of the Central Asian fold belt: mantle xenolith evidence. *Tectonophysics* **328**, 131–156.

Zhou M.-F., Malpas J., Song X.-Y., Robinson P. T., Sun M., Kennedy A. K., Lesher C. M., and Keays R. R. (2002) A temporal link between the Emeishan large igneous province (SW China) and the end-Guadalupian mass extinction. *Earth Planet. Sci. Lett.* **196**, 113–122.

Associate editor: Martin A. Menzies